

TITLE

Synaptonuclear messenger PRR7 inhibits c-Jun ubiquitination and regulates NMDA mediated excitotoxicity

Dana O. Kravchick¹, Anna Karpova⁴, Matous Hrdinka⁴, Jeffrey Lopez-Rojas⁴, Sanda Iacobas³, Abigail U. Carbonell¹, Dumitru A. Iacobas³, Michael R. Kreutz^{4,5} and Bryen A. Jordan^{1,2}.

¹Dominick P. Purpura Department of Neuroscience,

²Department of Psychiatry and Behavioral Sciences, Albert Einstein College of Medicine, Bronx, NY 10461, USA.

³Department of Pathology, New York Medical College, Valhalla, NY 10595, USA.

⁴Research Group Neuroplasticity, Leibniz Institute for Neurobiology, 39118 Magdeburg, Germany.

⁵Leibniz Group 'Dendritic Organelles and Synaptic Function', University Medical Center Hamburg-Eppendorf, Center for Molecular Neurobiology, Hamburg, Germany

Abbreviated Title: PRR7 inhibits c-Jun ubiquitination in neurons

Correspondence should be addressed to:

Bryen A. Jordan

Dominick P. Purpura Department of Neuroscience

Albert Einstein College of Medicine

1300 Morris Park Avenue

Rose Kennedy Center, Room 825

Bronx, NY 10461

Tel.: (718) 430-2675

E-mail: bryen.jordan@einstein.yu.edu

Keywords: Synapse-to-nucleus, ischemia, immediate early gene, FBW7, photoactivation,

Title: 102 characters (with spaces)

Number of figures: 6 Figures, 5 Supplementary, 2 tables

Abstract: 150 words

Introduction: 546 words

Discussion: 862 words

Total character count (with spaces, without references): 51581

ABSTRACT

Elevated c-Jun levels result in apoptosis and are evident in neurodegenerative disorders such as Alzheimer's disease and dementia and after global cerebral insults including stroke and epilepsy. NMDA receptor (NMDAR) antagonists block c-Jun upregulation and prevent neuronal cell death following excitotoxic insults. However, the molecular mechanisms regulating c-Jun abundance in neurons are poorly understood. Here we show that the synaptic component Proline Rich 7 (PRR7) accumulates in the nucleus of hippocampal neurons following NMDAR activity. We find that PRR7 inhibits the ubiquitination of c-Jun by E3 ligase SCF^{FBW7} (FBW7), increases c-Jun-dependent transcriptional activity and promotes neuronal death. Microarray assays show that PRR7 abundance is directly correlated with transcripts associated with cellular viability, and that PRR7 knockdown attenuates NMDAR-mediated excitotoxicity in neuronal cultures in a c-Jun dependent manner. Our results show that PRR7 links NMDAR activity to c-Jun function and provide new insights into the molecular processes that underlie NMDAR-dependent excitotoxicity.

INTRODUCTION

The transcription factor c-Jun is a principal component of the activator protein 1 (AP-1) complex, which is involved in the immediate early response following neuronal activity (Raivich & Behrens, 2006). To form the AP-1 complex, c-Jun can homo- or heterodimerize with members of the Fos or ATF families of transcription factors. AP-1 is required for neuronal survival and synaptic plasticity and has been implicated in seizures, addiction, pain and posttraumatic repair in the CNS (Alberini, 2009). Despite considerable interest in AP-1 biology, relatively little is known about how neuronal activity regulates c-Jun protein levels (Cruzalegui, Hardingham et al., 1999, Tischmeyer & Grimm, 1999). NMDAR activity increases c-Jun abundance in several neurodegenerative disorders and following ischemia or status epilepticus (Dragunow, Young et al., 1993, Herdegen, Skene et al., 1997, Zhang, Xu et al., 2006). In retina, excitotoxic NMDAR stimulation upregulates c-Jun mRNA and protein abundance (Munemasa, Ohtani-Kaneko et al., 2006a), and triggers c-Jun phosphorylation at amino acid residues 63/73 by activating c-Jun N-terminal kinases (JNK) (Coffey, 2014, Yang, Kuan et al., 1997). Phosphorylated c-Jun is transcriptionally active and can induce apoptosis via upregulation of cell death-inducing genes (Behrens, Sibilia et al., 1999, Ham, Babij et al., 1995, Song, Xie et al., 2011) **or by downregulating anti-apoptotic genes through repressor activity (Miao & Ding, 2003, Shaulian & Karin, 2002)**. Although numerous studies implicate c-Jun in apoptosis, its cellular function is context and stimulus dependent (Leppa & Bohmann, 1999) as c-Jun can also regulate axon regeneration and synaptic plasticity (Alberini, 2009, Hu, Levine et al., 2015).

In neurons, c-Jun protein levels are kept low by rapid proteasomal-mediated degradation to prevent cellular apoptosis (Nateri, Riera-Sans et al., 2004). The HECT-type E3-ligase Itch (Fang, Elly et al., 2002), MEKK1 (Xia, Wang et al., 2007) and RING type E3 ligase SCF^{FBW7} complex (composed of Skp1, Cullin1 and the F-box protein FBW7) (Nateri et al., 2004) can ubiquitinate and promote c-Jun proteasomal degradation. Ubiquitination by FBW7 requires c-Jun phosphorylation at Ser63/73 and Thr91/93. **NMDAR stimulation increases c-Jun phosphorylation and transcriptional activity by activating JNK (Schwarzschild, Cole et al., 1997). While MAPK-dependent phosphorylation can stabilize c-Jun expression in 3T3 cells (Musti, Treier et al., 1997), factors that protect c-Jun from polyubiquitination and degradation in neurons are unknown (Nateri et al., 2004).**

Several groups, including our own, identified PRR7 in mass-spectrometry based screens of postsynaptic densities (PSD) from rodent brains (Jordan, Fernholz et al., 2004,

Murata, Doi et al., 2005, Yoshimura, Yamauchi et al., 2004). PRR7 was found to interact with the membrane-associated guanylate kinase PSD95 via its C-terminal PDZ ligand, and associate with the NMDAR complex (Murata et al., 2005). PRR7 structure resembles that of transmembrane adaptor proteins (TRAPs) (Hrdinka, Draber et al., 2011), which mediate T-cell receptor signaling by assembling a membrane proximal signalosome. In Jurkat T-cells, expression of PRR7 triggers apoptotic cell death that is preceded by c-Jun upregulation, suggesting that PRR7 might regulate T-cell survival in a manner that involves c-Jun (Hrdinka et al., 2011).

Here we show that NMDAR stimulation increases PRR7 levels in the nucleus and that PRR7 inhibits FBW7-mediated c-Jun ubiquitination. We propose that PRR7 is a neuronal FBW7 inhibitor and a novel nuclear signaling molecule linking NMDAR activity to c-Jun function. **Moreover, we propose that PRR7 mediates NMDAR-mediated excitotoxicity in neuronal cultures in a c-Jun dependent manner.**

RESULTS

PRR7 expression and subcellular distribution in brain

Little is known about PRR7 expression in brain, so we first determined its tissue and developmental distribution. We found that PRR7 was highly expressed in the forebrain (Fig S1A) and showed strong developmental regulation, with expression evident at postnatal day 7 and plateauing ~4 weeks after birth (Fig S1B). This was similar to the developmental profiles of the NMDAR subunit GluN1 and PSD95, which correlates with synaptogenesis in rodent brains. Immunocytochemistry of rat primary hippocampal cultures at DIV21 showed that endogenous PRR7 had a punctate distribution throughout synaptodendritic compartments and colocalized with synaptic markers (Figs 1A-C, **S1C**). To determine the extent of synaptic colocalization, we performed triple colocalization analysis between PRR7, Bassoon and PSD95 (Fig 1B) and found that $38.8 \pm 3.6\%$ ($n=9$ neurons, p -value < 0.0001) of bona fide synapses (containing both PSD95 and Bassoon), contained PRR7. This suggests that PRR7 is abundant in some, but not all synaptic junctions. Exogenously expressed GFP-tagged PRR7 also colocalized with the synaptic marker Bassoon, corroborating imaging results of endogenous PRR7 distribution (Fig 1C). **PRR7 was also present in the soma and showed variable expression in the nucleus (Fig 1A, lower panels). Quantitation of PRR7 abundance throughout the neuron showed enriched, but significantly variable expression in nuclear and synaptic regions compared to perinuclear and dendritic regions (Fig S1C).**

Western blot analysis of subcellular fractions isolated from rat brains showed that PRR7 was markedly enriched in the PSD fraction, but was also present in purified nuclear fractions (Fig 1D).

NMDAR activation elevates PRR7 expression in the nucleus

PRR7 contains a putative lysine and arginine rich nuclear localization sequence (NLS) (KRR-RLR) near the N-terminus. Given immunocytochemical (Figs 1A, S1C) and Western blot (Fig 1D) evidence of both synaptic and nuclear PRR7, we determined if neuronal activity regulated the subcellular distribution of PRR7. Glutamate stimulation of rat DIV 21 primary hippocampal cultures increased PRR7 abundance in the nucleus (Fig 2A). This increase was also evident in the presence of the protein synthesis inhibitor cycloheximide, suggesting that it was not mediated by increased protein translation. **We also noted that glutamate stimulation led to elevated levels of PRR7 in the soma (Fig 2A). However, the increase in nuclear PRR7 was larger than the increase in somatic PRR7 as measured by an elevated ratio of nuclear to cytoplasmic PRR7 following stimulation (Fig S2D). These results are consistent with an activity-dependent nuclear import.** Glutamate stimulation also led to a concomitant reduction of PRR7 abundance at synapses that was not inhibited by the proteasome inhibitor epoxomicin (Fig 2B), suggesting that the decrease was not mediated by proteasomal degradation. To corroborate these results using another method, we treated high-density cortical cultures with glutamate and purified both synaptic and nuclear fractions from harvested cells (Fig S2A). As expected, glutamate stimulation led to an increase of PRR7 in the nucleus (Fig S2B) with a concomitant decrease at synapses (Fig S2C). To identify the specific ionotropic receptor activity required for this translocation, we treated neurons with glutamate in the presence of the NMDAR antagonist APV or the AMPAR antagonist CNQX. Only APV blocked the increase in nuclear PRR7 (Fig 2C). Neither CNQX nor the voltage-gated sodium channel blocker tetrodotoxin (TTX) blocked this process, suggesting that the accumulation of PRR7 in the nucleus did not require action potentials.

To assess the dynamics of PRR7 redistribution, we used Fluorescence Recovery After Photobleaching (FRAP) to track the nuclear accumulation of PRR7-GFP following NMDAR stimulation. PRR7-GFP was already present in the nucleus of non-stimulated cells with basal synaptic activity but was also prominently localized in dendrites and the soma (Figs 1C, 2D). We observed a rapid recovery of GFP fluorescence in photobleached nuclei in response to bath application of NMDA, indicating an activity-dependent nuclear import of PRR7 (Fig 2D, E). This import was not visible when we applied the NMDAR antagonist MK801 overnight and

during stimulation (Fig 2D,E). Treatment with MK801 significantly decreased basal PRR7-GFP fluorescence in the nucleus and soma (Fig 2D).

To confirm that PRR7 was translocating from distal dendrites into the nucleus, we transfected neurons with a PRR7 construct fused to the photoconvertible fluorescent protein mEos3 (Zhang, Chang et al., 2012b). Following expression of the fusion protein, we photoconverted PRR7-mEos in distal dendritic regions (ROIs) from green to red fluorescence and monitored accumulation of red-PRR7-mEos in the nucleus 30 minutes after stimulation with 50 μ M NMDA (Fig 2F, G). We found a robust increase in red-PRR7-mEos in the nucleus following treatment with NMDA, but not with MK801 (Fig 2F, G). These results, together with FRAP experiments and imaging and biochemical analyses of endogenous PRR7, strongly suggest that PRR7 translocates from synapses to nuclei following NMDAR activity.

PRR7 interacts with NMDARs in rat brain

Several activity dependent synapse-to-nucleus messengers bind to NMDARs (Jordan & Kreutz, 2009). We confirmed that PRR7 interacts with PSD95 and NMDARs in adult mouse brains (Murata et al., 2005) using co-immunoprecipitation experiments (Fig 3A). As PRR7 and NMDAR bind to different PDZ domains of PSD95 (Murata et al., 2005, Niethammer, Kim et al., 1996), we hypothesized that they might associate indirectly via PSD95. To clarify this, we first co-expressed GluN1 and a PRR7 construct with a C-terminal myc-tag blocking the PDZ ligand in HEK293 cells, which lack PSD95. However, PRR7 bound to GluN1 despite the blocked PDZ ligand, suggesting that PSD95 was not required (Fig 3B). This interaction was specific as PRR7 did not bind to the AMPAR subunits GluA1 or GluA2 (Fig 3C) and did not require the GluN2A or GluN2B subunits of NMDARs (Fig 3B). Binding to NMDARs was preserved under stringent conditions (RIPA buffer) and required the transmembrane domain (TM), the short N-terminus and 15 amino acids of the intracellular domain of PRR7 (Fig 3D).

We next asked whether PRR7 might have any effect on NMDA-mediated currents in HEK cells (Fig S3A, B) or in primary hippocampal neurons (Fig S3C). We found that PRR7 had no effect on NMDAR currents when co-expressed with NMDAR subunits in HEK cells (Fig S3A, B), irrespective of expressing GluN1 with GluN2A (Fig S3A) or GluN2B (Fig S3B). Moreover, shRNA-mediated knockdown of PRR7 had no effects on NMDA currents in primary hippocampal neurons (Fig S3C). We also assessed possible effects of PRR7 on miniature AMPAR-mediated currents. However, overexpression of PRR7 in cultured neurons neither modified the amplitude nor frequency of AMPAR-mediated currents (Fig S3E, F). Collectively these data do not support a role for PRR7 in regulating synaptic function.

As NMDAR activation resulted in an accumulation of PRR7 in the nucleus (Fig 2), we hypothesized that the interaction of PRR7 with GluN1 was modulated by NMDAR activity. We treated hippocampal cultured neurons with NMDA and found that this reduced the extent of PRR7-GluN1 interactions (Fig 3E). Together, our results suggest that PRR7 associates with GluN1 independent of PSD95 and dissociates from NMDARs following neuronal activity to allow for nuclear import.

PRR7 inhibits c-Jun ubiquitination

As PRR7 was shown to regulate c-Jun expression and phosphorylation (Hrdinka et al., 2011), we hypothesized that PRR7 could link NMDAR activity to c-Jun function. Therefore, we generated lentiviruses to knockdown (shRNAs) or overexpress PRR7 in primary neuronal cultures and found that PRR7 and c-Jun abundance were directly correlated. PRR7 knockdown decreased c-Jun abundance, while PRR7 overexpression increased c-Jun abundance (Fig 4A). **Neither overexpression nor knockdown of PRR7 altered c-Fos abundance (Fig 4A).** In HEK293 cells treated with cycloheximide, we found that PRR7 expression significantly increased c-Jun half-life (Fig 4B), suggesting that PRR7 inhibits c-Jun degradation. PRR7 contains a putative phosphodegron motif (VTPFLS) at amino acid 175, suggesting it may interact with the E3 ubiquitin ligase FBW7, which has been shown to ubiquitinate c-Jun in neurons (Nateri et al., 2004). To determine if PRR7 regulated c-Jun ubiquitination, we expressed FBW7 in HEK293 cells in the presence or absence of PRR7 and performed ubiquitination pulldown assays. We chose HEK293 cells because they do not express PRR7, have low amounts of FBW7 and express high amounts of c-Jun. We confirmed that FBW7 overexpression increased c-Jun ubiquitination (Fig 4C) as previously reported (Nateri et al., 2004). However, co-expression of FBW7 with PRR7 significantly blocked c-Jun ubiquitination (Fig 4C). To determine if PRR7 regulated c-Jun ubiquitination in neurons, we knocked down PRR7 in hippocampal neuronal cultures using lentiviral shRNAs and found that this led to increased c-Jun ubiquitination (Fig 4D). These results suggest that PRR7 inhibits c-Jun ubiquitination in neurons. PRR7 knockdown or overexpression had no effect on other FBW7 targets mTOR and Myc (Davis, Welcker et al., 2014) in neurons (Fig 4E), or in HEK293 cells (Fig S4). Taken together these results suggest that PRR7 specifically inhibits c-Jun ubiquitination and is not a general inhibitor of FBW7.

PRR7 forms a complex with c-Jun and FBW7

To determine why PRR7 specifically inhibited c-Jun ubiquitination, we tested whether these proteins interact. We found that PRR7 co-immunoprecipitated with c-Jun when

overexpressed in HEK293 cells (Fig 5A). Pull-down experiments *in vitro* using purified proteins demonstrated that these proteins interact directly (Fig 5B). The phosphodegron motif in PRR7 also suggested a direct interaction with FBW7. Indeed, PRR7 bound to FBW7 when overexpressed in HEK293 cells (Fig 5C), *in vitro* using purified proteins (Fig 5D), and also in rat brain lysates (Fig 5E). To determine if PRR7 blocked c-Jun ubiquitination by simple competition for FBW7 binding, we examined the interaction between PRR7, FBW7 and c-Jun in HEK293 cells. Surprisingly, PRR7 and FBW7 bound more strongly to c-Jun when both were cotransfected into heterologous cells (Fig 5F) suggesting that a c-Jun/FBW7/PRR7 complex is stabilized in the presence of all components. This points to a more complex mechanism of inhibition rather than simple substrate sequestration.

PRR7 regulates c-Jun dependent transcription and NMDA-dependent excitotoxicity

We hypothesized that regulating c-Jun ubiquitination would alter phosphorylated c-Jun levels (phospho-c-Jun) and thus c-Jun-dependent transcription, as phosphorylation of c-Jun enhances both its transcriptional activity and ubiquitination by FBW7 (Minden, Lin et al., 1995, Nateri et al., 2004). We found that PRR7 abundance was directly correlated with phospho-c-Jun (Serine 63) levels in primary hippocampal neurons (Fig 6A, black bars). As expected, PRR7 overexpression increased c-Jun transcriptional activity measured using an AP-1 reporter based luciferase assay in HEK293 cells (Fig 6B). **This increase in AP-1 transcriptional activity was likely mediated through changes in c-Jun alone, as c-Fos levels were not affected by PRR7 (Fig 4A).** To determine if PRR7 regulated gene expression in neurons, we performed microarray experiments on neuronal cultures transduced with control (NT), PRR7 knockdown (KD) or PRR7 overexpression (OE) lentiviruses. We compared the KD/NT to OE/NT values to control for the effects of viral infection. Results analyzed using Ingenuity Pathway Analysis (IPA) software (Ingenuity systems) revealed significant reciprocal changes in survival and cellular death pathways in response to PRR7 knockdown or overexpression, respectively (Fig 6C). The results also showed significant changes in c-Jun specific target genes predicting decreased cell survival in neurons overexpressing PRR7 (Fig S5). **Overall, manipulating PRR7 abundance significantly affected ~18% of RNAs analyzed (Tables S1, S2) and the full microarray dataset was deposited at the NCBI database at <http://www.ncbi.nlm.nih.gov/geo/query/acc.cgi?acc=GSE62686>.**

Given the microarray results, we next tested the effects of PRR7 on neuronal viability by overexpressing PRR7 in neuronal cultures and using propidium iodide staining (PI) *in situ* to identify dead cells. Expression of full length PRR7 (WT-PRR7-GFP) for 48h caused

substantial cell death compared to expression of GFP alone (Fig 6D). We compared WT-PRR7-GFP to **mNLS-PRR7-GFP** (**mutant nuclear localization sequence**), which is a full length-PRR7 protein mutated to contain five point substitutions within the NLS that substitutes lysine/arginine residues with alanine (K39A-R40A-R41A-R45A-R47A). **mNLS-PRR7-GFP** was not present in the nucleus following heterologous expression and did not cause cell death, suggesting that nuclear PRR7 was responsible for this effect (Fig 6D).

As PRR7 accumulates in the nucleus following NMDAR stimulation (Fig 2), we hypothesized that it may play a role in NMDAR-dependent excitotoxicity. To test this prediction, we first confirmed that glutamate stimulation increased c-Jun phosphorylation (Pozniak, Sengupta Ghosh et al., 2013) in primary hippocampal cultures (Fig 6A, gray bars) and found that this was blocked following PRR7 knockdown (Fig 6A). On the other hand, overexpression of PRR7 elevated phospho-c-Jun levels, but similar to PRR7 knockdown, abolished its regulation by glutamate stimulation. These results suggested that PRR7 inhibited the ubiquitination of phospho-c-Jun by FBW7. To explore the functional implications of this regulation, we examined the effects of PRR7 knockdown on NMDAR-mediated excitotoxicity. We treated neuronal cultures with NMDA (100 μ M, 25 min) and examined cell death using PI 14h later. Loss of PRR7 had no significant effect on cell survival in untreated neurons. However, PRR7 knockdown significantly reduced NMDA-triggered excitotoxicity compared to control neurons (Fig 6E). **These effects were not due to changes in NMDA or synaptic function as manipulating PRR7 abundance had no effect on NMDA or miniature AMPA mediated-currents in primary neuronal cultures (Fig S3).**

To determine if the neuroprotective effects of PRR7 knockdown required c-Jun, we used a cell permeable c-Jun inhibitor peptide that blocks c-Jun/JNK complex formation (Holzberg, Knight et al., 2003). We found that c-Jun inhibition partially rescued neurons from NMDAR-mediated excitotoxicity and that the extent of protection was similar to that obtained by PRR7 knockdown (Fig 6E). However, a combination of c-Jun inhibition and PRR7 knockdown did not have any additive effects (Fig 6E), suggesting that both c-Jun and PRR7 act through a similar signaling pathway. To further test this notion, we used a dominant negative c-Jun construct (c-Jun^{4A}) that cannot be phosphorylated (Nateri et al., 2004) or activated (Pulverer, Kyriakis et al., 1991, Smeal, Binetruy et al., 1991). As previously described (Estus, Zaks et al., 1994, Ham et al., 1995), overexpression of WT c-Jun led to high rates of neuronal cell death even in the absence of NMDA dependent stimulation (Fig 6F, black bars). Importantly, PRR7 knockdown partially rescued this effect, suggesting that PRR7

plays a role in c-Jun mediated neuronal death. While overexpression of c-Jun^{4A} did not cause neuronal death under control conditions (Fig 6F, gray bars), c-Jun^{4A} could partially rescue neurons from NMDAR-mediated excitotoxicity as expected from previous work (Behrens et al., 1999) (Fig 6F, gray bars, NMDA). However, this rescue was not additive with the effects of PRR7 knockdown (Fig 6F). Taken together, these results show that PRR7 mediates NMDAR-dependent excitotoxicity through the regulation of c-Jun function and that PRR7 knockdown has neuroprotective effects.

DISCUSSION

Here we show that PRR7 is a novel regulator of c-Jun ubiquitination and function in hippocampal neurons. Our data suggests that PRR7 is a synapse-to-nucleus messenger that links NMDAR activity to c-Jun dependent transcription by inhibiting its FBW7-mediated ubiquitination. This activity-dependent ubiquitination of a transcription factor represents an additional mechanism via which synaptic activity can regulate gene expression in neurons. Overall, this work provides new insights into NMDAR mediated neuronal excitotoxicity, which is associated with changes in total and phosphorylated c-Jun levels (Dragunow et al., 1993, Munemasa, Ohtani-Kaneko et al., 2006b).

Our data demonstrate an increase in nuclear PRR7 levels following glutamate stimulation that is not affected by inhibitors of proteasomal degradation or protein synthesis, thus implicating a transport process. Synapse-to-nucleus transport is supported by experiments using the monomeric photoswitchable fluorescent protein mEos (Wiedenmann, Ivanchenko et al., 2004, Zhang et al., 2012b), which show that photoconverted PRR7 at distal dendrites shuttles to the nucleus following stimulation with NMDA, and by FRAP experiments, which show that PRR7-GFP accumulates in the nucleus following activation of NMDAR.

However we did not detect a 'ring'-like pattern around the nucleus expected given the predicted transmembrane domain on PRR7 and given membrane bound proteins enter the nucleus via lateral diffusion (King, Lusk et al., 2006). Instead, PRR7 exhibits a diffuse and often punctate nuclear distribution. This suggests that either PRR7 is not membrane associated as predicted, or is released via limited proteolysis, which is a common mechanism in the transport of C-terminal fragments of transmembrane proteins including APP, N-Cadherin or protocadherins (Jordan & Kreutz, 2009). Alternatively, PRR7 may be associated with intranuclear lipid microdomains that bind DNA and protein complexes (Irvine, 2003). An

understanding of the mechanisms underlying the nuclear accumulation of PRR7 will require additional experiments.

The present work suggests that NMDAR activity leads to increased c-Jun phosphorylation because a rise in nuclear PRR7 inhibits the ubiquitination of phospho-c-Jun by FBW7. Therefore, we describe here an activity-dependent mechanism to regulate gene expression by inhibition of ubiquitination. This mechanism is different from others involved in activity-dependent changes in gene expression, which can rely on phosphorylation (CREB), nuclear translocation (NF- κ B, NFATc4) or upregulation (c-Fos) of transcription factors (West & Greenberg, 2011). Such a mechanism might keep phosphorylated c-Jun levels high for a short time window without requiring new transcription.

As an inhibitor of c-Jun ubiquitination, it was surprising that PRR7 forms a high affinity complex with FBW7 and c-Jun (Fig 5F). However, other inhibitors of FBW7 such as NEMO and Rack1 function in a similar way (Kim, Yang et al., 2010, Zhang, Zhu et al., 2012a). Rack1 blocks phospho-c-Jun ubiquitination by forming a high affinity ternary complex with FBW7 and *non-phosphorylated* c-Jun (Zhang et al., 2012a), which allows transcriptionally active phospho-c-Jun to escape degradation. This mechanism may provide specificity and thus spare alternative FBW7 substrates. Indeed, we have shown that PRR7 expression does not affect protein levels of the FBW7 substrates Myc and mTOR (Fig 4, S4). However, whether PRR7 can recruit phosphorylated or non-phosphorylated c-Jun into a complex with FBW7 is unclear at present.

While the present study implicates PRR7 in excitotoxicity, its neuronal function may be context-dependent as diverse synaptic stimuli differentially regulate neuronal processes (Dieterich, Karpova et al., 2008, Hardingham, Fukunaga et al., 2002b). For example, synaptic or extrasynaptic NMDAR activation result in the synapse-to-nucleus translocation of the CREB regulator Jacob (Dieterich et al., 2008, Karpova, Mikhaylova et al., 2013). However, synaptic activity leads to CREB phosphorylation and activation, while extrasynaptic activation of NMDARs triggers the CREB shutoff pathway and neuronal degeneration (Hardingham, Fukunaga et al., 2002a, Karpova et al., 2013). Cellular stress activates the AP-1 complex (Coffey, 2014) to promote either cell survival or apoptosis (Herdegen et al., 1997). As c-Jun has been implicated in synaptic plasticity and axon-regeneration (Alberini, 2009), other stimuli that regulate AP-1 transcription such as BDNF or plasticity inducing protocols (Gaiddon, Loeffler et al., 1996, Herdegen & Waetzig, 2001) may regulate PRR7 nuclear abundance.

Our microarray results predict a decrease in cell survival / viability in neurons overexpressing PRR7 (Fig 6C) that is strongly associated with changes in c-Jun specific target genes (Fig S5) including *Fos*, *Csf1r* and *Cdkn1b*. However, we also find changes in *Bdnf* as well as other transcripts controlled by CREB activity (Tao, Finkbeiner et al., 1998), which is not surprising given that CREB expression lies downstream of AP-1 transcriptional activity (Sanyal, Sandstrom et al., 2002). **Indeed, we find that the manipulation of PRR7 abundance results in extensive changes in the cellular transcriptome (Tables S1, S2), which illustrates how difficult it is to disentangle causality in transcriptional programs and microarray assays.**

To conclude, our study shows that PRR7 is an NMDAR-dependent nuclear messenger that regulates gene expression via inhibition of c-Jun ubiquitination. We demonstrate that the nuclear accumulation of PRR7 is necessary for its effects on cellular viability, suggesting that its effects on excitotoxicity involve the regulation of gene expression. To our knowledge this is the first evidence linking NMDAR activity to transcriptional control via regulation of ubiquitination. Moreover, the novel role for PRR7 as a messenger between pathological activation of NMDAR, increased c-Jun function and cell death provide insights into the molecular processes that underlie NMDAR-dependent excitotoxicity.

MATERIALS AND METHODS

Patch-clamp recordings in HEK293T cells and primary neurons

Cells were patched in the whole-cell mode as described previously (Karpova et al., 2013). The extracellular medium contained 145 mM NaCl, 2.5 mM KCl, 2 mM CaCl₂, 10 mM HEPES, 10 mM D-glucose, 1 μM TTX, 10 μM bicuculline and 10 μM CNQX in the experiments recording NMDA currents. In these experiments NMDA 100 μM and Glycine 10 μM, dissolved in extracellular solution, were puffed onto the soma. For experiments where AMPA-mediated mEPSCs were recorded, the extracellular solution contained 145 mM NaCl, 2.5 mM KCl, 2 mM MgCl₂, 2 mM CaCl₂, 10 mM HEPES, 10 mM D-glucose, 1 μM TTX, 10 μM Bicuculline and 10 μM APV. The intracellular solution contained in all cases 140 mM potassium gluconate, 10 mM EGTA, 10 mM HEPES, 2 mM MgCl₂, 1 mM CaCl₂, 4 mM NaATP and 0.4 mM GTP. Patch pipettes (3–5 MΩ) were pulled from thick-walled borosilicate glass tubing. Recordings were performed with an EPC9 patch-clamp amplifier. Data were acquired and stored using Patchmaster and analyzed with Fitmaster and GraphPad Prism. Patch-clamp recordings of primary neurons in the presence of NMDA were done at DIV21

while neurons were infected at DIV14. mEPSC amplitude and frequency were measured at DIV16 while neurons were infected at DIV11. HEK cells were transfected 2 days before recording.

Fluorescence Recovery After Photobleaching and photoconversion assay

All time-lapse experiments were performed on the upright SP5 CLSM system (Leica-Microsystems, Mannheim, Germany) equipped with Diode (405 nm), Argon (488 nm) and Diode Pumped Solid State (561 nm) lasers and images were taken with HCX APO L20x/1.00W objective (Leica, Germany). Quick change 18 mm chamber (**RC-41LP**, Warner Instruments) was used for mounting coverslips with neurons expressing PRR7-mEos on the microscope stage. We bleached GFP fluorescence in the nucleus by high argon laser (488nm) power and used a hybrid Detector (HyD) from Leica Microsystems (Wetzlar) to detect low expression levels of PRR7-GFP under low light excitation to prevent overexpression and phototoxicity artefacts. NMDA (50 μ M) was added directly to neurobasal medium immediately after acquisition of the frame t0. MK801 (10 μ M) and TTX (1 μ M) were kept in the medium overnight prior to and during data acquisition. Photoconversion experiments were performed as described previously (Dinamarca, Guzzetti et al., 2016). Distal dendrites, indicated as ROIs in 17-19 DIV primary hippocampal neurons expressing PRR7-mEos, were selected for photoconversion and illuminated with UV laser (405 nm) along the z-axis with a focal depth of 300–400 nm. After photoconversion, NMDA was added directly to the neurobasal culture media. For detection of photoconverted mEos, we used the hybrid Detector (HyD) from Leica Microsystems (Wetzlar).

Neuronal imaging and Propidium Iodide uptake cell death assay

Double colocalization analyses (JaCoP) and triple colocalization analyses (BlobProb) were performed using the respective add-ins in ImageJ (NIH) and as described previously (Klein, Younts et al., 2013). Quantitative analysis of immunocytochemistry experiments was performed blind to the stimulation used or identity of viruses used for infection. Dead cells in neuronal cultures co-expressing GFP, WT-PRR7-GFP or **mNLS-PRR7-GFP**, were stained with propidium iodide (1-2 mg/ml) added to culture medium 48 hours after transfection. All GFP-positive neurons were counted in each condition and either classified as dead (propidium iodide positive) or alive (propidium iodide negative). For excitotoxicity experiments, hippocampal cells were transduced with a control nontargeting shRNA (NT) or PRR7 shRNA

expressing viruses at DIV13 and were treated with 100 μ M NMDA at DIV21, chased for 14h and then imaged using propidium iodide. To inhibit c-Jun activity we used a cell permeable c-Jun peptide inhibitor (Tocris) that blocks JNK/c-Jun interactions (Holzberg et al., 2003). We added 100 μ M peptide 1 hour prior to NMDA stimulation as above. WT or 4A-cJun were transfected into neurons 12 hours prior to NMDA stimulation. Imaging of neurons and further analysis of cell death was carried out blind to the viral transduction and condition of treatment.

Cell cultures

Sprague–Dawley rats were killed using CO₂ according to the guidelines of the Albert Einstein College of Medicine Institutional Animal Care and Use Committee. Primary hippocampal neuronal cultures from embryonic day (18-19) embryos of either sex were prepared as described (Osten, Khatri et al., 2000). HEK293 cells were cultured in Dulbecco's modified Eagle's medium (DMEM, Gibco) supplemented with 10% v/v fetal bovine serum and antibiotics penicillin (100 U/ml) and streptomycin (100 μ g/ml). HEK293 cells were transfected using a standard calcium phosphate method. When overexpressing NMDAR subunits in HEK293 cells, the medium was supplemented with 500 μ M ketamine and 20 mM MgCl₂ after transfection to prevent NMDAR-induced cell death. High-density cortical cultures were prepared from rat embryos (day 18-19) and as described in Osten et al., 2000 with the modification of plating cells at a density of 50000 per cm².

Plasmids, antibodies and lentiviral vectors

We used pTRIP vectors to generate lentiviral shRNA vectors for knockdown following the methods previously described (Janas, Skowronski et al., 2006). The sequence used to knockdown PRR7 targeted the coding region of PRR7: 413bp [5'-CGGAATCGGACATGTCTAA 3']. To overexpress PRR7 we subcloned full length PRR7 into FUGW vector (Dittgen, Nimmerjahn et al., 2004). Viral particles were produced as described previously (Klein et al., 2013). Plasmids encoding human PRR7, PRR7-GFP, and PRR7(1-44)-GFP were generated previously (Hrdinka et al., 2011). FI-mNLS-PRR7-GFP (K39A-R40A-R41A-R45A-R47A) was generated employing PCR fast cloning followed by homologous recombination approach with the following primers: rev- 5'GCCTCCTCCTGGGCCGCTGCGAGGCGGCGGCAGG-3' and fw- 5'-GGCCCAGGAGGAGGCACTGGCCGAGCAGAACCTGCGC-3'. PRR7-mEos was generated by cloning full length PRR7 into the N-terminus of the monomeric EosFP protein mEos3.2

variant (Zhang et al., 2012b), which was a gift from Michael Davidson (Addgene plasmid # 54550). C-terminally tagged PRR7-Myc and PRR7-Flag construct were created by subcloning PRR7 into pRK-Myc and pFLAG-CMV vectors, respectively. The N-terminal deletion mutant PRR7 (34-269)-GFP was generated by PCR and inserted into pEGFP-C2 vector (Clontech). The rat GluN1 and GluN2B-Myc constructs were kindly provided by M. Horak (Prague). The rat GluA1, GluA2-Myc constructs were obtained from M. Heine (Magdeburg). We generated PRR7-myc-His plasmid by cloning full length PRR7 into pCDNA3.1 vector (Invitrogen). WT-cJun and 4A-cJun plasmids were a gift from Axel Behrens (Addgene plasmids #47443 and #47444). HA-tagged ubiquitin was a gift from Paul Lombroso (Yale University). pFlag-FBW7beta was a gift from Bruce Clurman (University of Washington). AP1(5x)Luc vector was a gift from George Wilding (University of Wisconsin). Antibodies used were: PRR7 (1:2000, Rb polyclonal; for imaging) a gift from Yoshinori Fujiyoshi (Nagoya University); and PRR7 (1:1000, mouse monoclonal; Thermo Scientific) both were previously described (Hrdinka et al., 2011, Murata et al., 2005). Additional antibodies used were: GluN1 (1:1000, Chemicon); Shank (1:1000; UC Davis/NIH NeuroMab Facility); GAPDH (1:5000; GeneTex); SNAP25 (1:1000, abcam); Fibrilarin (1:500; Developmental Studies Hybridoma Bank, University of Iowa); c-Myc (sc-40; 1:2000; Santa Cruz); c-Jun (1:1000; Cell Signaling Technology); phospho-c-Jun (60A8 targeting Serine 63; 1:1000; Cell Signaling Technology); HA (1:2000; Thermo Scientific); Flag (M2; 1:5000; Sigma-Aldrich); Poly-Ubiquitin K-GG (GX41; 1:1000; Lucerna); GFP (B34; 1:2000; Covance); PSD95 (K28/43; 1:1000, UC Davis/NIH NeuroMab Facility); Synaptic Vesicle 2 (SV2; 1:150 Developmental Studies Hybridoma Bank, University of Iowa), MAP2 (1:1000; EncoreBio) and Bassoon (1:1000; Synaptic Systems).

Subcellular Fractionation

Fractionation of synaptic and nuclear as well as other cellular compartments were carried as previously described (Klein et al., 2013).

Ubiquitination assay

HEK293 cells were transfected with HA-Ubiquitin, Flag-FBW7 with or without PRR7 or PSD95 as a control. In neuronal cultures we knocked down PRR7 in primary hippocampal cultures from DIV10-17. 24h after transfection in HEK293 cells or 7 days following viral transduction in neurons, cells were treated with MG132 for 4h and lysed with 2% SDS, 50mM

Tris pH 8.0, boiled for 5 min and sonicated. Lysates were then diluted 10 fold with 1% Triton X-100, 75mM NaCl, 10% glycerol, 2mM EDTA, 50mM Tris pH 8.0 and rocked at 4°C for 1h. 1 µg of c-Jun antibody was then added overnight at 4°C and immunoprecipitation (IP) was carried out according to standard procedures. Following the IP, eluates were subjected to SDS-PAGE and Western blots carried out using anti-HA antibodies (in cells) or poly-Ub antibody (in neurons). Western blot quantifications were done by densitometry using ImageJ.

Microarray

We have used our optimized protocol (Iacobas, Iacobas et al., 2013) to cohybridize differently labeled biological replicas with each array (“multiple yellow” strategy (Soares, de Lima et al., 2010)) of Agilent rat two-color gene expression 4x44k arrays. Total RNA was extracted with Qiagen RNeasy mini-kit, concentration determined with a NanoDrop ND-2000 Spectrophotometer and purity with Agilent RNA 6000 Nano kit in an Agilent 2100 Bioanalyzer. Total RNA was reverse transcribed in the presence of Cy3/Cy5 dUTP and the incorporation of the fluorescent tags was determined with the NanoDrop. The arrays were scanned with an Agilent G2539A dual laser scanner and primary analysis performed with (Agilent) Feature Extraction 11.1 software. All spots affected by local corruption or with foreground fluorescence less than twice the background were disregarded and data normalized and analyzed following our standard procedure (Iacobas et al., 2013). The gene expression data complying with the “Minimum Information about Microarray Experiments” (MIAME) were deposited at <http://www.ncbi.nlm.nih.gov/geo/query/acc.cgi?acc=GSE62686>

IPA Analysis

Microarray results considered as significantly changed between NT and KD or OE conditions were such that showed a 1.5-fold difference between the samples and exhibited a p -value<0.05. Activation Z-score was calculated by IPA software and represents a significance measure that predicts the activation states of transcriptional regulators or the trend of a biological process. Functional analyses of KD and OE (Fig 6C) were organized by ascending values Z-score and opposing trend of the KD analysis. All the functional analyses and upstream activation networks were generated through the use of QIAGEN’s Ingenuity Pathway Analysis (IPA®QIAGEN Redwood City, www.qiagen.com/ingenuity).

Luciferase assay

~70,000 HEK293 cells were transfected with 50ngs of AP1(5x)Luc, pEGFP, and PRR7mycHis or PSD95mycHis (as control). Luciferase luminescence was measured 24h following transfection using a Beckman DTX800 Microplate reader and normalized to GFP fluorescence to account for variability in transfection efficiency.

Statistical analysis

Student t-test was carried out for comparison of two groups. Comparison of more than two groups was carried out using one-way ANOVA using multiple comparisons where appropriate. Post-hoc testing of ANOVA was selected based on conditions and indicated in the figure legends. Two-way ANOVA was used in cases where two variables were introduced (e.g., treatment and infection). For all figs, *p*-values of comparison between experimental results are depicted as follows: **p* < 0.05, ***p* < 0.01, ****p* < 0.001, *****p* < 0.0001. “n.s.” indicates a *p*-value > 0.05. All values are presented as mean ± s.e.m and all reported % values are compared to controls.

ACKNOWLEDGEMENTS

This work was supported by NIH grants AG039521 (B.A.J), 5R01HL092001 (D.A.I), SFB 779 TP B08 (M.R.K and A.K.), SFB 854 TP7 and DFG Kr1879/5-1, 6-1 (M.R.K) and NIMH training fellowship 5F31MH095381 (D.O.K). Flag tagged FBW7 and rat GluA1, GluA2-Myc constructs plasmids were kindly provided by Dr. Bruce Clurman and Dr. Martin Heine, respectively. AP-1 luciferase plasmid was generously provided by Dr. George Wilding. Rabbit PRR7 antibody was provided by Dr. Yoshinori Fujiyoshi.

AUTHOR CONTRIBUTIONS

D.O.K., A.K, M.H., J.L.R., A.U.C, M.R.K and B.A.J. designed and performed all the biochemical and imaging experiments and analyzed the data; S.I., D.A.I, and D.O.K. performed and analyzed the microarray assays. D.O.K., M.R.K. and B.A.J wrote the paper.

CONFLICT OF INTEREST

The authors declare no competing financial interests.

REFERENCES

- Alberini CM (2009) Transcription factors in long-term memory and synaptic plasticity. *Physiol Rev* 89: 121-45
- Behrens A, Sibilio M, Wagner E (1999) Amino-terminal phosphorylation of c-Jun regulates stress-induced apoptosis and cellular proliferation. *Nature genetics* 21: 326-329
- Coffey ET (2014) Nuclear and cytosolic JNK signalling in neurons. *Nat Rev Neurosci* 15: 285-99
- Cruzalegui FH, Hardingham GE, Bading H (1999) c-Jun functions as a calcium-regulated transcriptional activator in the absence of JNK/SAPK1 activation. *EMBO J* 18: 1335-44
- Davis RJ, Welcker M, Clurman BE (2014) Tumor suppression by the Fbw7 ubiquitin ligase: mechanisms and opportunities. *Cancer Cell* 26: 455-64
- Dieterich DC, Karpova A, Mikhaylova M, Zdobnova I, Konig I, Landwehr M, Kreutz M, Smalla KH, Richter K, Landgraf P, Reissner C, Boeckers TM, Zuschratter W, Spilker C, Seidenbecher CI, Garner CC, Gundelfinger ED, Kreutz MR (2008) Caldendrin-Jacob: a protein liaison that couples NMDA receptor signalling to the nucleus. *PLoS Biol* 6: e34
- Dinamarca MC, Guzzetti F, Karpova A, Lim D, Mitro N, Musardo S, Mellone M, Marcello E, Stanic J, Samaddar T, Burguiere A, Caldarelli A, Genazzani AA, Perroy J, Fagni L, Canonico PL, Kreutz MR, Gardoni F, Di Luca M (2016) Ring finger protein 10 is a novel synaptonuclear messenger encoding activation of NMDA receptors in hippocampus. *Elife* 5
- Dittgen T, Nimmerjahn A, Komai S, Licznarski P, Waters J, Margrie TW, Helmchen F, Denk W, Brecht M, Osten P (2004) Lentivirus-based genetic manipulations of cortical neurons and their optical and electrophysiological monitoring in vivo. *Proc Natl Acad Sci U S A* 101: 18206-11
- Dragunow M, Young D, Hughes P, MacGibbon G, Lawlor P, Singleton K, Sirimanne E, Beilharz E, Gluckman P (1993) Is c-Jun involved in nerve cell death following status epilepticus and hypoxic-ischaemic brain injury? *Brain Res Mol Brain Res* 18: 347-52
- Estus S, Zaks WJ, Freeman RS, Gruda M, Bravo R, Johnson EM, Jr. (1994) Altered gene expression in neurons during programmed cell death: identification of c-jun as necessary for neuronal apoptosis. *J Cell Biol* 127: 1717-27
- Fang D, Elly C, Gao B, Fang N, Altman Y, Joazeiro C, Hunter T, Copeland N, Jenkins N, Liu YC (2002) Dysregulation of T lymphocyte function in itchy mice: a role for Itch in TH2 differentiation. *Nat Immunol* 3: 281-7
- Gaiddon C, Loeffler JP, Larmet Y (1996) Brain-derived neurotrophic factor stimulates AP-1 and cyclic AMP-responsive element dependent transcriptional activity in central nervous system neurons. *J Neurochem* 66: 2279-86
- Ham J, Babij C, Whitfield J, Pfarr C, Lallemand D, Yaniv M, Rubin L (1995) A c-Jun dominant negative mutant protects sympathetic neurons against programmed cell death. *Neuron* 14: 927-939
- Hardingham G, Fukunaga Y, Bading H (2002a) Extrasynaptic NMDARs oppose synaptic NMDARs by triggering CREB shut-off and cell death pathways. *Nature neuroscience* 5: 405-414
- Hardingham GE, Fukunaga Y, Bading H (2002b) Extrasynaptic NMDARs oppose synaptic NMDARs by triggering CREB shut-off and cell death pathways. *Nat Neurosci* 5: 405-14
- Herdegen T, Skene P, Bahr M (1997) The c-Jun transcription factor--bipotential mediator of neuronal death, survival and regeneration. *Trends Neurosci* 20: 227-31
- Herdegen T, Waetzig V (2001) AP-1 proteins in the adult brain: facts and fiction about effectors of neuroprotection and neurodegeneration. *Oncogene* 20: 2424-2437

Holzberg D, Knight CG, Dittrich-Breiholz O, Schneider H, Dorrie A, Hoffmann E, Resch K, Kracht M (2003) Disruption of the c-JUN-JNK complex by a cell-permeable peptide containing the c-JUN delta domain induces apoptosis and affects a distinct set of interleukin-1-induced inflammatory genes. *J Biol Chem* 278: 40213-23

Hrdinka M, Draber P, Stepanek O, Ormsby T, Otahal P, Angelisova P, Brdicka T, Paces J, Horejsi V, Drbal K (2011) PRR7 is a transmembrane adaptor protein expressed in activated T cells involved in regulation of T cell receptor signaling and apoptosis. *J Biol Chem* 286: 19617-29

Hu JY, Levine A, Sung YJ, Schacher S (2015) cJun and CREB2 in the postsynaptic neuron contribute to persistent long-term facilitation at a behaviorally relevant synapse. *J Neurosci* 35: 386-95

Iacobas DA, Iacobas S, Chachua T, Goletiani C, Sidyelyeva G, Veliskova J, Velisek L (2013) Prenatal corticosteroids modify glutamatergic and GABAergic synapse genomic fabric: insights from a novel animal model of infantile spasms. *J Neuroendocrinol* 25: 964-79

Irvine RF (2003) Nuclear lipid signalling. *Nat Rev Mol Cell Biol* 4: 349-60

Janas J, Skowronski J, Van Aelst L (2006) Lentiviral delivery of RNAi in hippocampal neurons. *Methods Enzymol* 406: 593-605

Jordan BA, Fernholz BD, Boussac M, Xu C, Grigorean G, Ziff EB, Neubert TA (2004) Identification and verification of novel rodent postsynaptic density proteins. *Mol Cell Proteomics* 3: 857-71

Jordan BA, Kreutz MR (2009) Nucleocytoplasmic protein shuttling: the direct route in synapse-to-nucleus signaling. *Trends Neurosci* 32: 392-401

Karpova A, Mikhaylova M, Bera S, Bar J, Reddy PP, Behnisch T, Rankovic V, Spilker C, Bethge P, Sahin J, Kaushik R, Zuschratter W, Kahne T, Naumann M, Gundelfinger ED, Kreutz MR (2013) Encoding and transducing the synaptic or extrasynaptic origin of NMDA receptor signals to the nucleus. *Cell* 152: 1119-33

Kim BY, Yang JS, Kwak SY, Zhang XK, Han YH (2010) NEMO stabilizes c-Myc through direct interaction in the nucleus. *FEBS Lett* 584: 4524-30

King MC, Lusk CP, Blobel G (2006) Karyopherin-mediated import of integral inner nuclear membrane proteins. *Nature* 442: 1003-7

Klein ME, Younts TJ, Castillo PE, Jordan BA (2013) RNA-binding protein Sam68 controls synapse number and local beta-actin mRNA metabolism in dendrites. *Proc Natl Acad Sci U S A* 110: 3125-30

Leppa S, Bohmann D (1999) Diverse functions of JNK signaling and c-Jun in stress response and apoptosis. *Oncogene* 18: 6158-62

Miao ZH, Ding J (2003) Transcription factor c-Jun activation represses mdr-1 gene expression. *Cancer Res* 63: 4527-32

Minden A, Lin A, Claret FX, Abo A, Karin M (1995) Selective activation of the JNK signaling cascade and c-Jun transcriptional activity by the small GTPases Rac and Cdc42Hs. *Cell* 81: 1147-57

Munemasa Y, Ohtani-Kaneko R, Kitaoka Y, Kumai T, Kitaoka Y, Hayashi Y, Watanabe M, Takeda H, Hirata K, Ueno S (2006a) Pro-apoptotic role of c-Jun in NMDA-induced neurotoxicity in the rat retina. *J Neurosci Res* 83: 907-18

Munemasa Y, Ohtani-Kaneko R, Kitaoka Y, Kumai T, Kitaoka Y, Hayashi Y, Watanabe M, Takeda H, Hirata K, Ueno S (2006b) Pro-apoptotic role of c-Jun in NMDA-induced neurotoxicity in the rat retina. *Journal of neuroscience research* 83: 907-918

Murata Y, Doi T, Taniguchi H, Fujiyoshi Y (2005) Proteomic analysis revealed a novel synaptic proline-rich membrane protein (PRR7) associated with PSD-95 and NMDA receptor. *Biochemical and biophysical research communications* 327: 183-191

Musti AM, Treier M, Bohmann D (1997) Reduced ubiquitin-dependent degradation of c-Jun after phosphorylation by MAP kinases. *Science* 275: 400-2

Nateri A, Riera-Sans L, Da Costa C, Behrens A (2004) The ubiquitin ligase SCFFbw7 antagonizes apoptotic JNK signaling. *Science (New York, NY)* 303: 1374-1378

Niethammer M, Kim E, Sheng M (1996) Interaction between the C terminus of NMDA receptor subunits and multiple members of the PSD-95 family of membrane-associated guanylate kinases. *J Neurosci* 16: 2157-63

Osten P, Khatri L, Perez JL, Kohr G, Giese G, Daly C, Schulz TW, Wensky A, Lee LM, Ziff EB (2000) Mutagenesis reveals a role for ABP/GRIP binding to GluR2 in synaptic surface accumulation of the AMPA receptor. *Neuron* 27: 313-25

Pozniak C, Sengupta Ghosh A, Gogineni A, Hanson J, Lee S-H, Larson J, Solanoy H, Bustos D, Li H, Ngu H, Jubb A, Ayalon G, Wu J, Searce-Levie K, Zhou Q, Weimer R, Kirkpatrick D, Lewcock J (2013) Dual leucine zipper kinase is required for excitotoxicity-induced neuronal degeneration. *The Journal of experimental medicine*

Pulverer BJ, Kyriakis JM, Avruch J, Nikolakaki E, Woodgett JR (1991) Phosphorylation of c-jun mediated by MAP kinases. *Nature* 353: 670-4

Raivich G, Behrens A (2006) Role of the AP-1 transcription factor c-Jun in developing, adult and injured brain. *Progress in neurobiology* 78: 347-363

Sanyal S, Sandstrom DJ, Hoeffer CA, Ramaswami M (2002) AP-1 functions upstream of CREB to control synaptic plasticity in *Drosophila*. *Nature* 416: 870-4

Schwarzschild MA, Cole RL, Hyman SE (1997) Glutamate, but not dopamine, stimulates stress-activated protein kinase and AP-1-mediated transcription in striatal neurons. *J Neurosci* 17: 3455-66

Shaulian E, Karin M (2002) AP-1 as a regulator of cell life and death. *Nature cell biology* 4: 6

Smeal T, Binetruy B, Mercola DA, Birrer M, Karin M (1991) Oncogenic and transcriptional cooperation with Ha-Ras requires phosphorylation of c-Jun on serines 63 and 73. *Nature* 354: 494-6

Soares MB, de Lima RS, Rocha LL, Vasconcelos JF, Rogatto SR, dos Santos RR, Iacobas S, Goldenberg RC, Iacobas DA, Tanowitz HB, de Carvalho AC, Spray DC (2010) Gene expression changes associated with myocarditis and fibrosis in hearts of mice with chronic chagasic cardiomyopathy. *J Infect Dis* 202: 416-26

Song B, Xie B, Wang C, Li M (2011) Caspase-3 is a target gene of c-Jun:ATF2 heterodimers during apoptosis induced by activity deprivation in cerebellar granule neurons. *Neurosci Lett* 505: 76-81

Tao X, Finkbeiner S, Arnold DB, Shaywitz AJ, Greenberg ME (1998) Ca²⁺ influx regulates BDNF transcription by a CREB family transcription factor-dependent mechanism. *Neuron* 20: 709-26

Tischmeyer W, Grimm R (1999) Activation of immediate early genes and memory formation. *Cellular and molecular life sciences : CMLS* 55: 564-574

West AE, Greenberg ME (2011) Neuronal activity-regulated gene transcription in synapse development and cognitive function. *Cold Spring Harb Perspect Biol* 3

Wiedenmann J, Ivanchenko S, Oswald F, Schmitt F, Rocker C, Salih A, Spindler KD, Nienhaus GU (2004) EosFP, a fluorescent marker protein with UV-inducible green-to-red fluorescence conversion. *Proc Natl Acad Sci U S A* 101: 15905-10

Xia Y, Wang J, Xu S, Johnson GL, Hunter T, Lu Z (2007) MEKK1 mediates the ubiquitination and degradation of c-Jun in response to osmotic stress. *Mol Cell Biol* 27: 510-7

Yang DD, Kuan CY, Whitmarsh AJ, Rincon M, Zheng TS, Davis RJ, Rakic P, Flavell RA (1997) Absence of excitotoxicity-induced apoptosis in the hippocampus of mice lacking the *Jnk3* gene. *Nature* 389: 865-70

Yoshimura Y, Yamauchi Y, Shinkawa T, Taoka M, Donai H, Takahashi N, Isobe T, Yamauchi T (2004) Molecular constituents of the postsynaptic density fraction revealed by proteomic analysis using multidimensional liquid chromatography-tandem mass spectrometry. *J Neurochem* 88: 759-68

Zhang J, Zhu F, Li X, Dong Z, Xu Y, Peng C, Li S, Cho YY, Yao K, Zykova T, Bode A, Dong Z (2012a) Rack1 protects N-terminal phosphorylated c-Jun from Fbw7-mediated degradation. *Oncogene* 31: 1835-1844

Zhang M, Chang H, Zhang Y, Yu J, Wu L, Ji W, Chen J, Liu B, Lu J, Liu Y, Zhang J, Xu P, Xu T (2012b) Rational design of true monomeric and bright photoactivatable fluorescent proteins. *Nat Methods* 9: 727-9

Zhang QG, Xu YL, Li HC, Han D, Zhang GY (2006) NMDA receptor/L-VGCC-dependent expression and AMPA/KA receptor-dependent activation of c-Jun induced by cerebral ischemia in rat hippocampus. *Neurosci Lett* 398: 268-73

FIGURE LEGENDS

Fig 1- Synaptic and nuclear localization of PRR7.

(A) Upper panels- Immunofluorescence imaging of PRR7 with Shank (synaptic) and MAP2 (dendritic) markers in DIV21 hippocampal neurons. Lower panels- Single plane apotome images of nuclei (DAPI) show PRR7 can be present (arrow) or absent (arrowhead) from nuclei.

(B) Synaptic and dendritic distribution of PRR7 and pre (Bassoon) and postsynaptic (PSD95) markers (arrowheads-triple colocalization).

(C) PRR7-GFP expressed in 17DIV hippocampal neurons is present in dendritic spines (arrows). **Scale bar is 15 μ m.**

(D) PRR7 distribution across subcellular fractions (TOT = whole lysate, Syn = synaptosomes, Nuc = nuclei) isolated from rat hippocampal tissue. Fib (Fibrillarin), SNAP25 and PSD95 were used as nuclear, presynaptic and postsynaptic markers, respectively.

Fig 2- NMDAR activation regulates PRR7 subcellular distribution.

(A) Immunocytochemical analyses show that glutamate stimulation (Glut, 100 μ M 5 min + 25 min washout) increased PRR7 in the nucleus. **Cycloheximide (100 μ M) added 30 min prior to glutamate stimulation did not affect this increase (Cont=100 \pm 12.5%, Glut=202.1 \pm 15.2%; +cycloheximide Cont=104.9 \pm 3.6, Glut=231.4 \pm 10.9) (n \sim 30-50 cells).**

(B) Decreased synaptic PRR7 immunostaining following glutamate stimulation in DIV 21 hippocampal neurons. **Epoxomicin (50 nM) added 20 min prior to stimulation did not affect this decrease (Cont=100 \pm 3.6%, Glut=32.3 \pm 1.3%; +epoxomicin Cont=99.8 \pm 4.6,**

Glut=42.9±1.1). (n=14-17 dendrites, >1200 puncta for each group). Statistical analyses for (A) and (B) were performed using the Mann Whitney test.

(C) Quantification of nuclear PRR7 immunostaining in cultured hippocampal neurons.

Treatments (APV [50 µM, APV-(2R)-amino-5-phosphonovaleric acid], CNQX [40 µM, 6-cyano-7 nitroquinoxaline-2,3-dione], TTX [1 µM, tetrodotoxin], NMDA [50 µM, N-Methyl-D-Aspartate]) as indicated. Only APV treatment blocked the glutamate dependent increase in nuclear PRR7 (108.1 ± 19%). Statistical significance was determined using one-way ANOVA in conjugation with Sidak post-hoc test.

(D) PRR7-GFP accumulates in the nucleus of hippocampal neurons upon NMDA treatment.

Depicted are representative averaged confocal images (30x30 µm²) from optical sections (300 nm step size) of PRR7-GFP expressing neurons (DIV17) before and after bleaching. Prior to stimulation there was substantial PRR7-GFP in the nucleus due to basal neuronal activity (upper panel). This was reduced by incubation overnight with MK801 (10 µM) and TTX (1 µM) (lower panel). NMDA (50 µM) stimulation, but not MK-801, led to recovery of nuclear PRR7-GFP fluorescence following bleaching of nuclear ROIs at t₀' (blue arrow in E).

(E) Quantification of changes in nuclear GFP fluorescent intensities were normalized to time point t₀' and corrected for bleaching. No significant differences in PRR7-GFP FRAP were found in control (MK801) conditions. GFP intensities are displayed via look-up-table (LUT). Data are represented as mean±SEM; n=9 cells (NMDA) and n=5 cells (MK801). Analysis was done using one-way ANOVA using Bonferroni post-hoc correction.

(F) PRR7-mEos translocates from distal dendrites to the nucleus upon NMDA treatment. (Left panels) Confocal maximal intensity projection images of hippocampal neurons expressing PRR7-mEos before and after photoconversion of distal dendrites (ROIs) through the image z-stack from green (488nm) to red (568nm) using a UV laser (405 nm). (Right panels) Averaged intensity projection images from nuclear planes showing accumulation of photoconverted PRR7-mEos (568nm) in the nucleus following NMDA stimulation (50 µM-30min).

(G) Paired quantification of changes in background corrected fluorescent intensities of nuclear PRR7-mEos at 0 min and 30 min following NMDA stimulation or MK801 treatment. (Average increase; NMDA=617.8±47.7%, n=11 cells, p<0.0005; MK801=206.1±13.6%, n=5 cells, n.s.). Statistical significance was determined by two-way ANOVA using Sidak's correction for multiple comparisons.

Fig 3- PRR7 binding to GluN1 is regulated by NMDAR activity. (A) Co-Immunoprecipitations (Co-IPs) of PRR7 with GluN1, PSD95 and GluN2B from rat brain lysates. FT = flowthrough, IgG = normal IgGs. (B) Co-IPs from HEK293 cells of c-terminal myc-tagged PRR7 with GluN1 in the absence of other NMDAR subunits or PSD95. (C) Co-IPs from HEK293 cells transfected with tagged NMDA or AMPA receptor subunits and PRR7 (myc-tagged GluN2B and GluA2 and flag-tagged PRR7). (D) (top) Schematics of the different PRR7 constructs used for co-IP (FL= full length). (bottom) PRR7 deletion constructs and NMDAR subunits were expressed in HEK293 cells and Co-IPs performed as indicated. (E) Co-IPs of PRR7 with GluN1 from high-density primary neuronal cultures following treatment with NMDA (100 μ M, 30 min, representative of n=4).

Fig 4- PRR7 inhibits c-Jun ubiquitination.

(A) Western blots of lysates of primary neurons transduced with control lentiviruses (NT) or lentiviruses to knockdown (KD) or overexpress (OE) PRR7. PRR7 knockdown reduced ($75.6 \pm 6.9\%$) while PRR7 overexpression (OE) increased ($157.6 \pm 22.8\%$) c-Jun levels compared to controls. **No change was detected in c-Fos levels. One-way ANOVA test was used to analyze results with Dunett's post hoc test** (n=16 gels for c-Jun and 4 gels for c-Fos).

(B) Control or PRR7 transfected HEK293 cells were treated with cycloheximide for the indicated time points and c-Jun protein levels were measured by Western blotting. PRR7 expression significantly stabilized c-Jun levels at 120 min ($110.0 \pm 7.5\%$ vs control $68.7 \pm 7.9\%$) and 240 minutes ($83.6 \pm 5.2\%$ vs control $43.7 \pm 3.4\%$). Values for c-Jun were normalized to their respective 0 min time point (n=4 gels for each group performed blind). **T-tests between similar time points were used to analyze results.**

(C) PRR7, FBW7 and/or a control protein (PSD95) were transfected into HEK293 cells and c-Jun ubiquitination was measured by immunoprecipitating c-Jun and blotting for ubiquitin. Ubiquitination of c-Jun in the presence of FBW7 ($178.3 \pm 26.9\%$) was significantly reduced in the presence of PRR7 ($103.7 \pm 20.6\%$) but not a control protein (PSD95) (n=5 gels for all groups).

(D) Western blots of c-Jun ubiquitination in hippocampal primary neuronal cultures. PRR7 knockdown (KD) elevated ($149 \pm 10.62\%$, n=6 gels) c-Jun ubiquitination level in comparison to control neurons (NT). **Statistical significance was determined by t-test.**

(E) Western blots showing knockdown (KD) or overexpression (OE) of PRR7 in primary hippocampal neurons do not alter levels of other FBW7 targets mTOR or Myc. **Significance**

for (C) and (E) were determined using two-way ANOVA with Dunnett's post-hoc test. Data is presented as mean \pm sem. All % values represent comparisons to control.

Fig 5- PRR7 interacts with c-Jun and the E3 ubiquitin ligase FBW7.

(A) Co-IPs of PRR7 with c-Jun from lysates of HEK293 cells overexpressing PRR7.

(B) Pulldown assays *in vitro* using purified proteins showed a direct interaction between PRR7 and c-Jun.

(C) Co-IPs of PRR7 with FBW7 from lysates of HEK293 cells overexpressing PRR7 and FBW7.

(D) Pulldown assays *in vitro* using purified PRR7 and FBW7.

(E) Co-IPs of endogenous PRR7 and FBW7 from lysates of rat brain.

(F) Co-IPs of PRR7 with c-Jun and FBW7 from lysates of HEK293 cells overexpressing PRR7 and FBW7. FBW7 expression increased the amount of c-Jun pulled down with PRR7 (n=4 gels for each panel, representative blots). Lower bar graphs- quantitation for Western blots show c-Jun/FBW7 binding is 41.4 \pm 13.9% greater in the presence of PRR7 (normalized for FBW7 expression). Similarly, c-Jun/PRR7 binding is 97.4 \pm 38.1% greater in the presence of FBW7 (normalized for PRR7 expression). Statistical significance was calculated using unpaired t-tests.

Fig 6- PRR7 regulates c-Jun transcriptional activity and mediates NMDAR-dependent excitotoxicity.

(A) Western blots of phospho-c-Jun in primary neuronal cultures. Quantification of phospho-c-Jun represents a ratio of phospho-c-Jun to total c-Jun and all ratios were normalized to NT. PRR7 knockdown (KD) decreased, while PRR7 overexpression (OE) increased phospho-c-Jun levels (black bars). Glutamate stimulation (gray bars) increased phospho-c-Jun/c-Jun ratio in NT but not in KD or OE neurons (n=7 gels for all groups). Significance was determined using two-way ANOVA with Sidak post-hoc test.

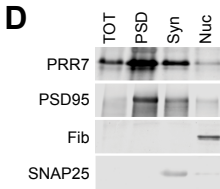
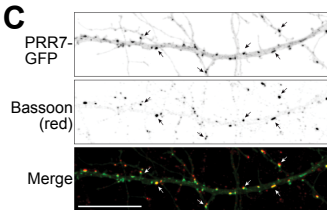
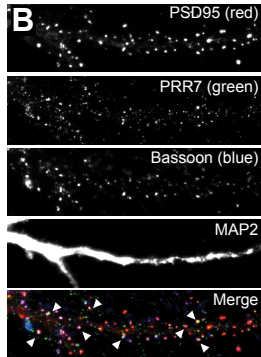
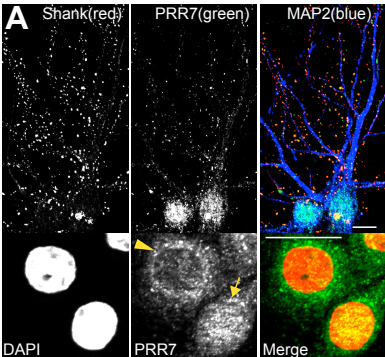
(B) AP-1 driven luciferase luminescence assays. PRR7 expression in HEK293 cells increased AP-1 activity (190.6 \pm 13.9%, n=12; RLU= relative light units). Statistical significance was determined using t-tests.

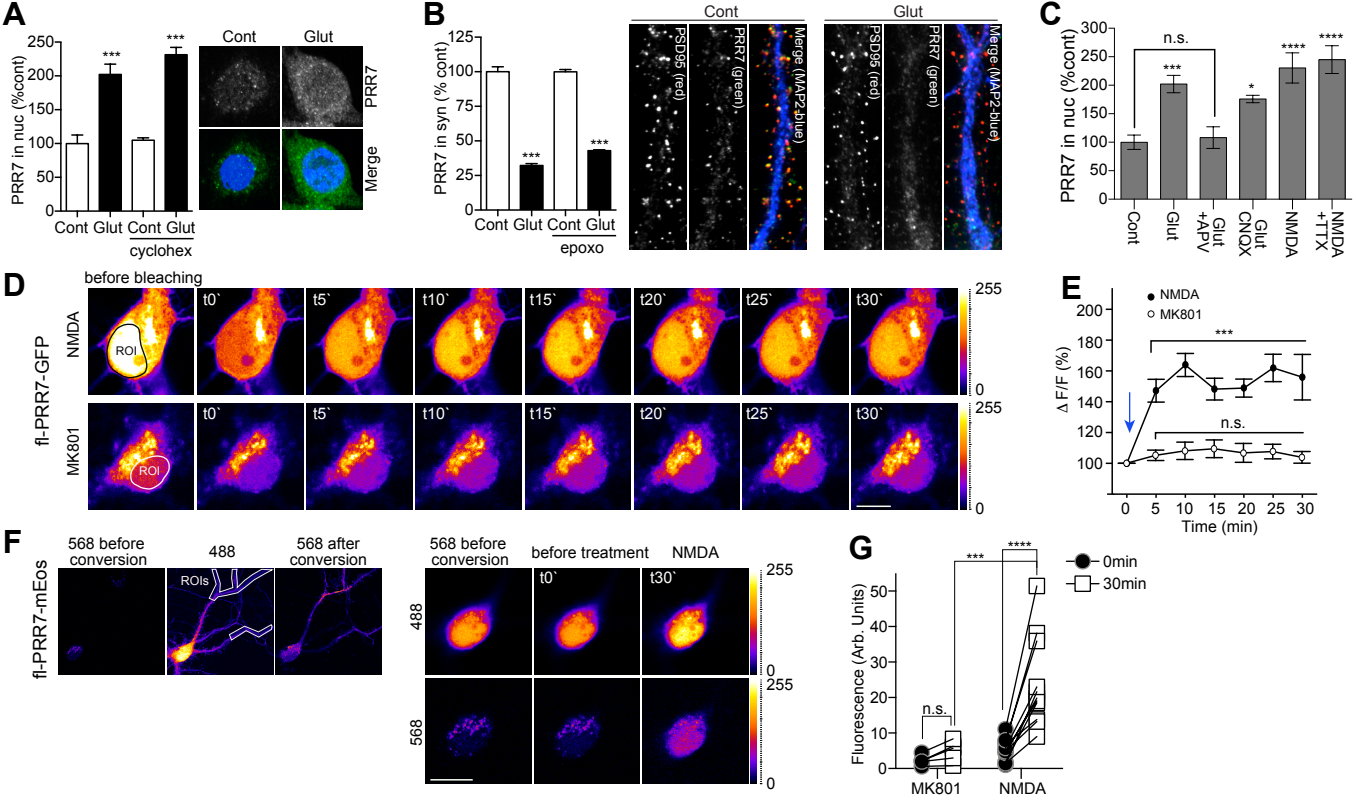
(C) Ingenuity Pathway Analysis (IPA)-predicted cellular functions based on microarray analysis. Functions are sorted by p-value (Highest-top).

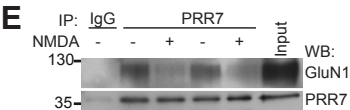
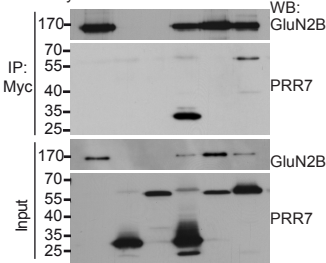
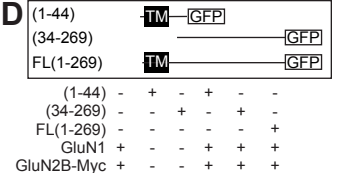
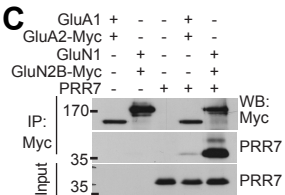
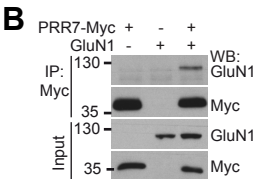
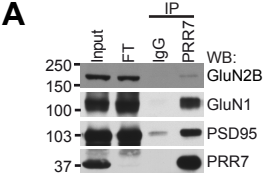
(D) Quantitation of cell death using 30 minutes of PI *in-situ* staining following 48h of WT-PRR7-GFP or mNLS-PRR7-GFP overexpression in primary hippocampal neuronal cultures (n=24 cells per group). Images represent a max projection of five z-stack sections across the cell body.

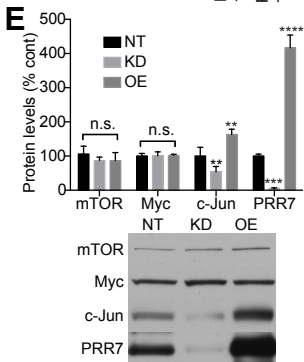
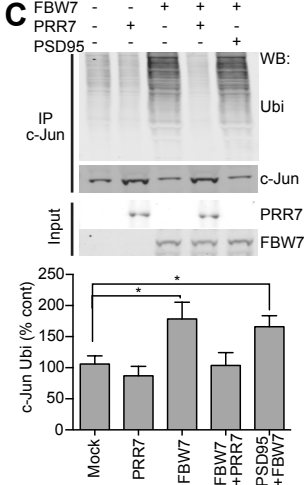
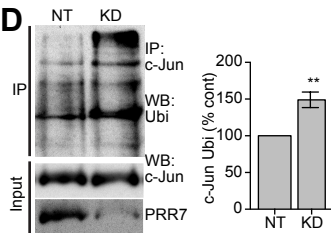
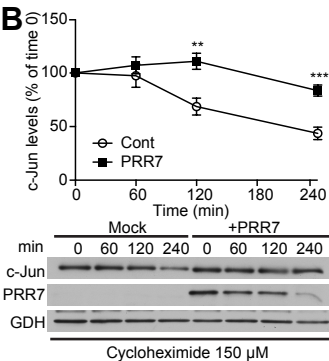
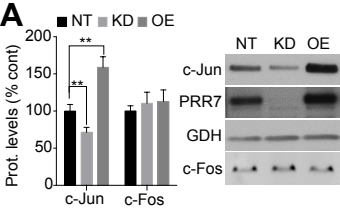
(E) NMDA treatment (25 min, 100 μ M followed by 14h chase) caused $83.6 \pm 3.5\%$ cell death in control neurons compared to $60.3 \pm 4.6\%$ cell death in neurons with PRR7 expression knocked down. A c-Jun inhibitory peptide reduced NMDA-mediated cell death to $66.2 \pm 6.0\%$ in control neurons and to $55.6 \pm 5.3\%$ in neurons knocked down for PRR7, but this difference was not statistically significant (n=5 independent experiments). Two-way ANOVA was used in conjunction with Tukey post-hoc test. (Left) Representative images showing transduced neurons (green- GFP) and PI staining (red).

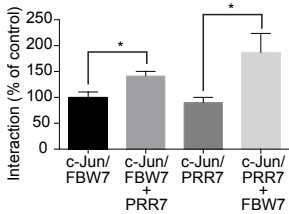
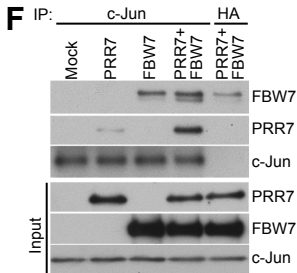
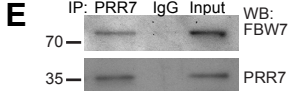
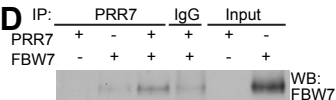
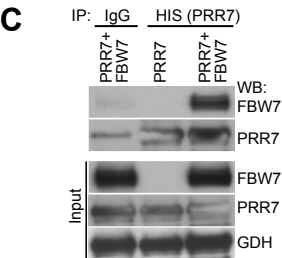
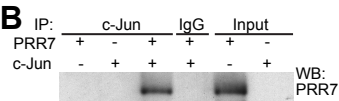
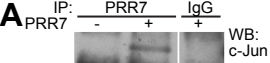
(F) Quantification of cell death in response to NMDA stimulation in the presence or absence of PRR7 and either WT c-Jun or a dominant negative c-Jun^{4A} (4A). Overexpression of WT c-Jun caused extensive neuronal cell death ($84.8 \pm 2.4\%$) that was reduced in neurons knocked down for PRR7 ($43.8 \pm 9.2\%$). Overexpressing 4A conferred neuroprotection to NMDA excitotoxicity ($50.8 \pm 7.9\%$) but was not additive with PRR7 knockdown ($42.3 \pm 8.1\%$) (n=3 independent experiments). Significance was determined using two-way ANOVA in conjunction with Tukey post-hoc test. Images are representative 10X widefield micrographs showing transduced neurons (green- GFP) and PI staining (red). Data is presented as mean \pm sem. All % values represent comparisons to control.

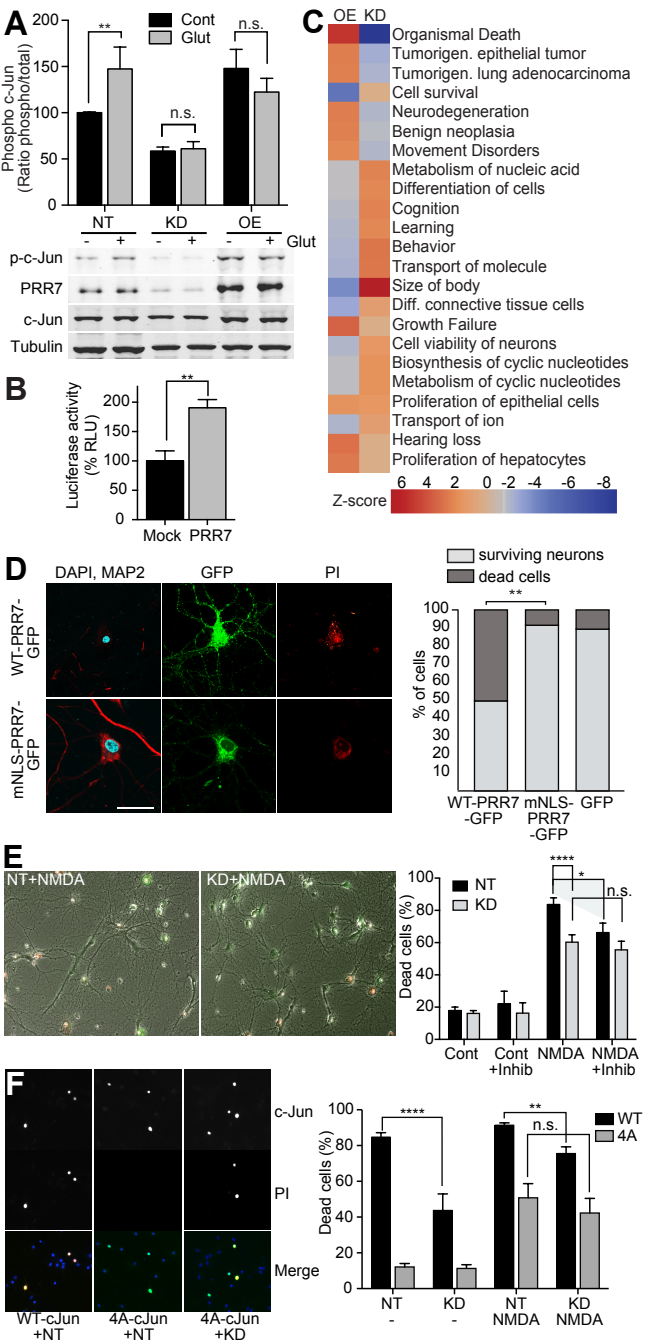






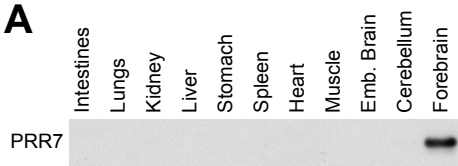




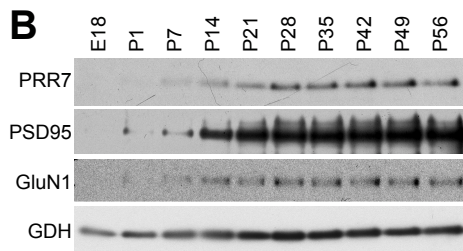


Supplemental Figures and legends

A



B



C

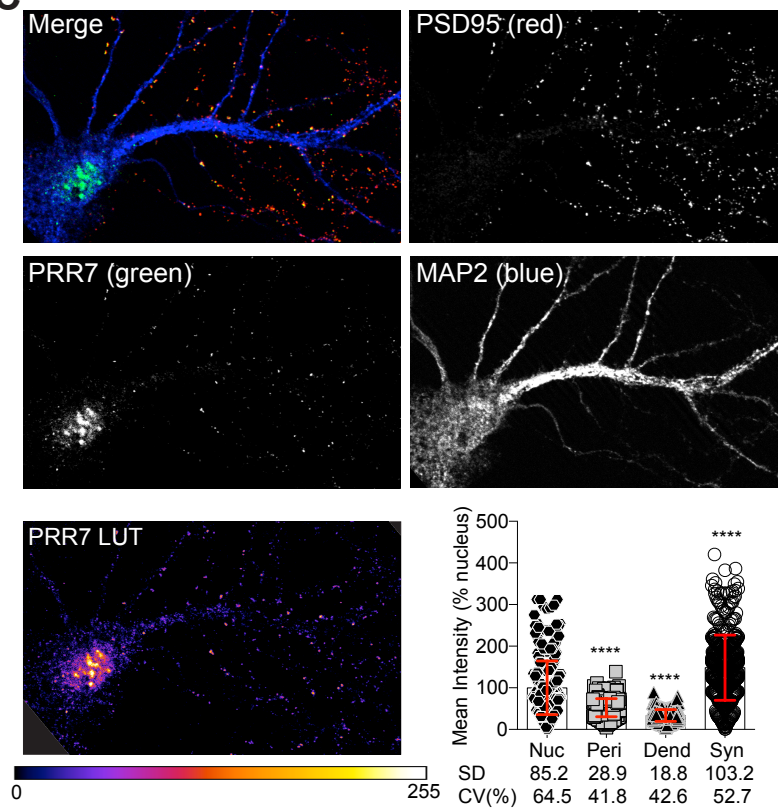


Fig S1 - Tissue expression of PRR7.

(A) Different rat tissue lysates analyzed by Western blotting. **Forebrain included cortex and hippocampus only. All tissues were dissected from adult rats 3-6 months of age.**

(B) Western blots of rat brain lysates from the indicated ages show the PRR7 developmental profile compared to that of PSD95 and GluN1 subunits. GDH (GAPDH) was used as a loading control.

(C) **Imaging and quantification of PRR7 intensity at randomly selected puncta in nuclear (Nuc-colocalized with DAPI), perinuclear (Peri-adjacent to DAPI), dendritic (Dend-colocalized with MAP2) and synaptic (Syn-colocalized with PSD95) regions. Bottom left- representative image of PRR7 intensity using fire lookup table (scale below) in a cultured pyramidal hippocampal neuron DIV 21. Bar graphs show all data points, normalized to nuclear intensity. Statistical analysis was done using one-way ANOVA with Tukey's post hoc test. Standard deviation (SD) and coefficient of variation (CV%) values displayed below show significant variability in nuclear and synaptic localizations. n=14 neurons, ~300 puncta for each region. Data represent mean \pm SD (red error bars).**

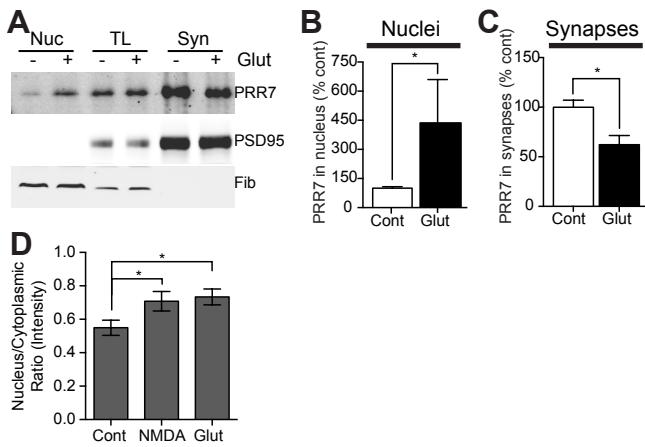


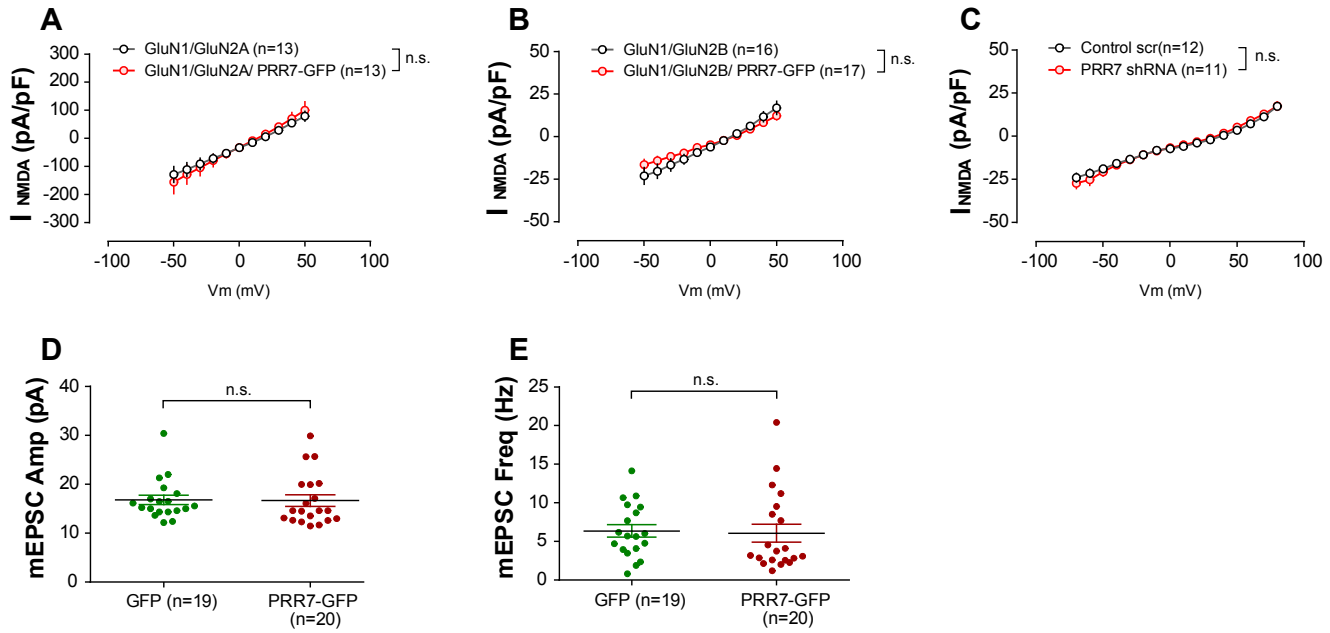
Fig S2 - NMDAR activation regulates PRR7 subcellular distribution.

(A) Western blots of nuclei, total fraction (TL) and synaptosome protein extracts isolated from high-density cortical cultures depicting PRR7 levels as well as a synaptic (PSD95) and nuclear (fibrillarin-Fib) markers.

(B) Quantifications of nuclear and (C) synaptic PRR7 levels following glutamate stimulation.

Glutamate stimulation increased nuclear ($436.3 \pm 223\%$, $n=7$ gels) and decreased synaptic ($62.2 \pm 9.3\%$, $n=6$ gels) PRR7 levels. Statistical significance was determined using Mann-Whitney tests.

(D) Quantification of nuclear and somatic PRR7 expression in neuronal cells cultures. Glutamate or NMDA stimulation increased Nucleus/Cytoplasmic ratios (based on integrated density; mean intensity X area) from 0.55 ± 0.04 (Cont) to 0.71 ± 0.06 (NMDA) and 0.73 ± 0.05 (Glut) ($n=18-33$ cells per group). Statistical significance was determined using unpaired t-tests as shown.



Fig

S3. PRR7 does not significantly modify NMDA or miniature AMPA mediated-currents. NMDA currents in HEK cells and primary cultured hippocampal neurons were recorded in a whole-cell configuration. NMDA 100 μM and Glycine 10 μM were puffed through a pipette oriented towards the cell soma in a Mg^{2+} - free extracellular solution. Overexpression of PRR7 in HEK cells, together with NMDAR subunits GluN1 and GluN2A (A) or GluN1 and GluN2B (B), did not significantly modify evoked NMDA currents when compared to control conditions (in the absence of PRR7). (C) Knockdown of endogenous PRR7 did not change evoked NMDA currents in primary cultured hippocampal neurons. (D) The amplitude and frequency (E) of AMPA-mediated miniature excitatory postsynaptic currents (mEPSCs) from primary cultured hippocampal neurons were not significantly different between cells overexpressing PRR7 and control cells overexpressing GFP.

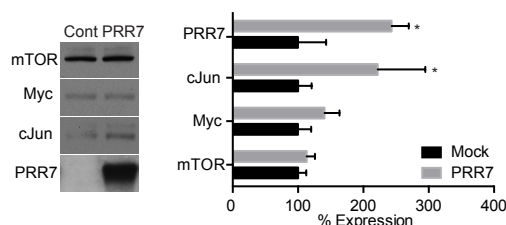


Fig S4 - PRR7 is a specific inhibitor of FBW7 mediated c-Jun ubiquitination. Western blots of lysates from control and PRR7 expressing HEK293 cells. PRR7 expressing HEK293 cells showed no difference in mTOR or myc levels compared to controls. **Statistical analysis was carried out using two-way ANOVA with Sidak's post hoc test.**

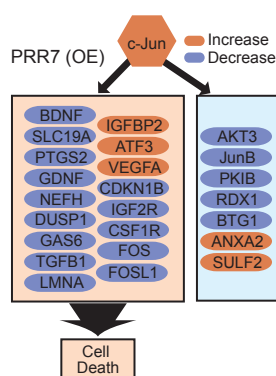


Fig S5 – Microarray assay show changes in c-Jun target genes. Ingenuity Pathway Analysis (IPA)-predicted cellular functions based on microarray analysis (full results deposited <http://www.ncbi.nlm.nih.gov/geo/query/acc.cgi?acc=GSE62686>) show that significant changes in c-Jun target genes predict decreased cell survival in OE neurons (p -value $5.07E-14$). **Both increased and decreased targets can reflect increased c-Jun activity as c-Jun acts both as a repressor and promoter of gene transcription.**

Table S1- Heat map of alphabetically ordered regulated genes. The background color indicates the fold change (negative for down-regulation) of that gene in the profiled sample with respect to the average expression level in the NT condition (neurons transduced with viruses expressing non-targeting shRNAs [NT], viruses to knockdown PRR7 [KD], viruses to overexpress PRR7 [OE] and no viral infection [NO]). The map was limited to the genes that exhibit significant regulation with respect to NT in at least one other condition (NO, KD or OE).

Table S2- List of significantly regulated Unigenes. Genes listed with abbreviations, fold-change (Ex. NT/NO), p -value significance (Ex. P -NT/NO) and overall change (Green, D = downregulated; Red, U = upregulated). Separate pages are shown for ratios between NT/NO, KD/NT and OE/NT.